Journal of the Nigerian Association of Mathematical Physics
Volume **23 (March, 2013), pp313 – 324**

The Effect Of Water Solubles In Radiative Forcing Of Urban Aerosols

[1]Tijjani B. I. and [2]Akpootu D. O.
[1]Department of Physics,
Bayero Univerisity, Kano,
[2]Department of Physics,
Usmanu Danfodiyo University, Sokoto.

Abstract

In this paper we model the effect of water soluble (WS) in the radiative forcing (RF) of urban aerosols at spectral range of 0.25 to 1.00 μm at relative humidities (RHs) (0, 50, 70, 80, 90, 95, 98 and 99%) using OPAC. The concentrations of WS used were 15,000 20,000, 25,000, 30,000 and 35,000 cm^{-3}. These parameters were used to determine the Radiative forcing (RF) . The RF decreases with wavelength at RH 0 to 90% in a form of power law but quadratic in concave form at RH 95 to 99%. The effect of RH on RF (cooling) increases with the increase in RH. The effect of adding WS is such that the RF at longer wavelength becomes more linear and started curving as from 30,000cm^{-3} and the cooling increases with the increase in concentration and RH. Using regression analysis, the Angstrom exponents were determined along with α_1 and α_2, the coefficients of a second order polynomial fit. The α increases with RH from 0% to 90% and decreases from 95 to 99% at concentration 15,000, 20,000, and 25,000, but at 30,000 and 35,000cm^{-3} it increases from 0 to 80% and decreases from 90 to 99%.

1.0 Introduction

The effects of aerosols on climate can be large and complex due to the fact that aerosols chemical composition, abundance and size distribution are highly variable both spatially and temporally [1]. Aerosol particle types which contribute to the scattering coefficient include organic particles, water-soluble inorganic species such as sulphates, nitrates etc. that are produced by conversion from SO_2 and NO_x associated mainly with fossil fuel/biomass combustion, and ammonium from fertilizers and biological sources. Most of the earliest investigations on direct aerosol forcing have focused on sulphate aerosol because of their importance as an anthropogenic aerosol component [2,3]. Sulphate particle is an important component of atmospheric aerosols. Sulphate makes up a substantial fraction of tropospheric aerosol in both urban and remote/rural areas [4,5,6]. Sulphate aerosols are capable of modifying the climate not only by scattering incoming sunlight back to space (direct effect) but also by altering the properties of clouds(indirect effect) [1].

The water-soluble part of aerosol particles originates from gas to particle conversion can consists of various kinds of sulfates, nitrates, such as salts like ammonium hydrogen sulphate (NH_4HSO_4), ammonium nitrate (NH_4NO_3) and ammonium sulphate ($(NH_4)_2SO_4$) and organic acids like formic, acetic, pyruvic and oxalic acids. Similarly, high concentrations of sulfate aerosols are expected from the oxidation of SO_2 that is emitted by diesel-fueled mobile sources and from the numerous coal-fired industries and power generation stations located both in urban areas and the heavy commercial vessel traffic in these areas is also a significant source of SO_2 [7,8]. Thus it contains more than only the sulfate aerosol that is often used to describe anthropogenic aerosol. The mass density of sulfate is about half that of the water-soluble components. This component is also used to model the di-methyl sulfiderelated aerosol produced over the oceans [9].

Understanding the influence of atmospheric aerosol on climate, visibility and photochemistry requires accurate data of aerosol optical properties such as the light extinction coefficient, single scattering albedo, upscatter fraction, and size distribution which are necessary for estimating direct aerosol radiative forcing on climate [10-13].

Aerosol optical properties can be strongly dependent upon relative humidity (RH). Hygroscopic properties of soluble atmospheric particles significantly influence the size of the particles at ambient relative humidity, and thus influence the scattering capability, optical depth and residence time of these particles in the atmosphere [14].This is because water uptake affects aerosol atmospheric lifetime, particle size and composition, which in turn affect direct radiative forcing of climate because of its influence by hygroscopic growth of the aerosols [15-17]. For these reasons, hygroscopic data are also required to calculate microphysical aerosol properties such as size distribution or optical depth at ambient conditions.

In this paper we modeled the effect of water soluble by changing their concentrations of WS using OPAC at eight relative

Corresponding author: ***B. I. Tijjani,*** E-mail: idrith@yahoo.com, Tel. +234 8037030877

humidities (0, 50, 70, 80, 90, 95, 98 & 99%). The optical properties used in this paper are, optical depths, single scattering albedos and asymmetric parameters. They were used to calculate the radiative forcing, and the Ångström coefficient which characterizes the dependence of AOD on wavelength and provides information about the size of aerosol particles. The asymmetric parameters were analysed to ascertain the nature of the RF because of the nature of the forward scattering.
The models extracted from OPAC are given in Table 1.

Table 1 Compositions of aerosol types [9].

Components	Model1 (N_i,cm^{-3})	Model2 (N_i,cm^{-3})	Model3 (N_i,cm^{-3})	Model4 (N_i,cm^{-3})	Model5 (N_i,cm^{-3})
Insoluble	1.50	1.50	1.50	1.50	1.50
water soluble	15,000.00	20,000.00	25,000.00	30,000.00	35,000.00
Soot	110,000.00	110,000.00	110,000.00	110,000.00	110,000.00
Total	**125,001.50**	**130,001.50**	**135,001.50**	**140,001.50**	**145,001.50**

Where N_i is the number of particles cm^{-3}.
Although a fully exact radiative transfer model is difficult, so in this paper we used the approach of [18] where they show that the direct aerosol radiative forcing at the top of the atmosphere can be approximated by

$$\Delta F_R = -\frac{S_0}{4} T_{atm}^2 (1 - N_{cloud}) 2\tau\{(1-A)^2\beta\omega - 2A(1-\omega)\} \quad (1)$$

Where S_0 =1368Wm^{-2} is a solar constant, T_{atm} =0.79 is the transmittance of the atmosphere above the aerosol layer, N_{cloud}=0.6 is the fraction of the sky covered by clouds, the global averaged albedo A=0.22 over land, β is the fraction of radiation scattered by aerosol into the atmosphere and τ is the optical thickness and ω is the single scattering albedo [19]. The above expression gives the radiative forcing due to the change of reflectance of the earth-aerosol system. The upscattering fraction is calculated using an approximate relation [20]

$$\beta = \frac{1}{2}(1 - g) \quad (2)$$

where g is the asymmetry parameter. Although the model is simple but was used to provide sresonable estimates for the radiative forcing by both sulfate aerosols [2] and absorbing smoke aerosols [18].
The spectral behavior of the aerosol optical thickness, with the wavelength of light (λ) is expressed as inverse power law [21]:

$$\tau(\lambda)=\beta\lambda^{-\alpha} \quad (3)$$

where β is the turbidity and α is the Angstrom exponent [22,23]. The formula is derived on the premise that the extinction of solar radiation by aerosols is a continuous function of wavelength, without selective bands or lines for scattering or absorption [24]. The wavelength dependence of τ(λ) can be characterized by the Angstrom parameter, which is a coefficient of the following regression:

$$\ln\tau(\lambda) = -\alpha\ln(\lambda) + \ln\beta \quad (4)$$

The Angstrom exponent itself varies with wavelength, and a more precise empirical relationship between aerosol extinction and wavelength is obtained with a 2nd-order polynomial [25 -34] as:

$$\ln\tau(\lambda) = \alpha_2(\ln\lambda)^2 + \alpha_1\ln\lambda + \ln\beta \quad (5)$$

Here, the coefficient α_2 accounts for a "curvature" often observed in sunphotometry measurements. In case of negative curvature (α_2<0, convex type curves) the rate of change of α is more significant at the longer wavelengths, while in case of positive curvature (α_2>0, concave type curves) the rate of change of α is more significant at the shorter wavelengths [30, 26, 28, 35]. Eck et al. [26] reported the existence of negative curvatures for fine-mode aerosols and positive curvatures for significant contribution by coarse-mode particles in the size distribution.

RESULTS AND OBSERVATIONS

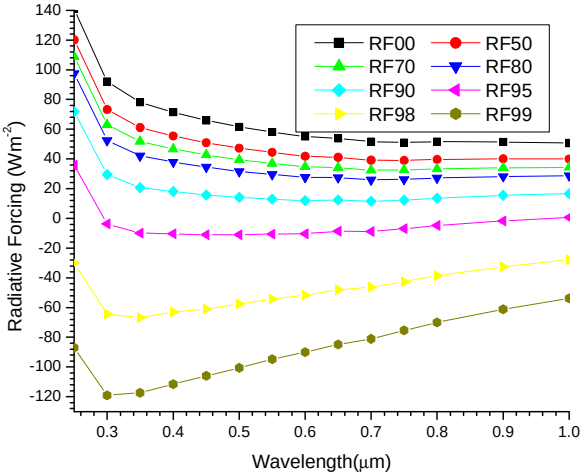

Figure 1a. A graph of radiative forcing against wavelength for model1 at RHs 0, 50, 70, 80, 90, 95, 98 and 99%

The graph shows that RF behaves as inverse power law with wavelength at RHs 0 to 70% RH but started curving upward (concave) at higher wavelengths from 80% and the curving continues to increase upto 99%. Its relation with RH is that RF(cooling) increases with the increase in RHs. The nature of the graphs with RH reflects the dominance of fine particles.

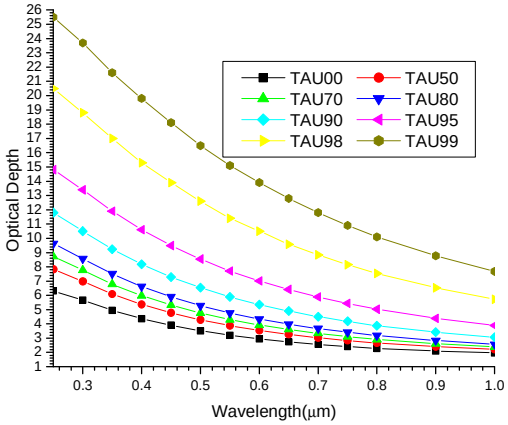

Figure 1b. A graph of optical depth against wavelength for model1at RHs 0, 50, 70, 80, 90, 95, 98 and 99%.

Figure 1b shows that optical depths follow a relatively smooth decrease with the increase in wavelengths though some are steeper than others and the steepness increases with the increase in RHs. It is evident from the figure that there is a relatively strong wavelengths dependence of optical depths at shorter wavelengths that decreases toward longer wavelengths irrespective of the RH, attributing to the presence of fine and coarse particles. The presence of fine mode particles which are selective scatters enhanced the irradiance scattering in shorter wavelength only while the coarse mode particles provide similar contributions to the optical depths at both wavelengths [36]. Additionally fine particles scatter more lights in the forward direction than coarse particles.

In relation to RH, it shows that optical depths increase with the increase in RH. As the RH increases there is an increase in hygroscopic growth more to fine particles than coarse particles and since fine particles scatter more lights in the forward direction than coarse particles, that is why also the optical depth are higher at shorter wavelengths than longer wavelengths even at higher RHs. These hygroscopic growth behaviors also reveal an immense potential of light scattering enhancement in the forward direction at high RHs and the potential of fine particles to be highly effective cloud condensation nuclei. The increase of AOD with RH at the delequicence point (95 to 99%) is that the growth increase substantially, making the process strongly nonlinear with RH [37, 38].

It also shows monomode type of particle size distributions in the form of Junge power law in this spectral range [26] and increase in RH has caused increase in mode growth because of the increase in optical depths.

Table 2 The results of the Angstrom coefficients for Model1 using equations (4) and (5) at the respective relative humidities using regression analysis with SPSS16.0.

	Linear			Quadratic			
RH(%)	R^2	α	β	R^2	α_1	α_2	β
0	0.99716	0.88942	1.89869	0.99718	-0.87478	0.01074	1.90477
50	0.99767	0.95463	2.18600	0.99807	-1.01951	-0.04759	2.15528
70	0.99731	0.97719	2.37797	0.99839	-1.08704	-0.08058	2.32166
80	0.99666	0.99232	2.59259	0.99868	-1.14479	-0.11185	2.50777
90	0.99444	1.00563	3.15204	0.99913	-1.24161	-0.17311	2.99387
95	0.99054	0.99513	4.10309	0.99951	-1.31856	-0.23726	3.82356
98	0.98330	0.94069	6.21860	0.99982	-1.35728	-0.3056	5.67836
99	0.97709	0.88316	8.44252	0.99991	-1.34429	-0.33827	7.63453

Table 2 shows that at 0% RH the value of α from the linear part reflects the dominance of coarse particles, and the quadratic part also verifies this because $\alpha_2>0$. However as the RH increased from 50 to 90% the value of α continues to increase and α_2 becomes negative and its magnitude continues to increase with the increase in RH which indicates the increase in the dominance of fine particles with the increase in RH.

At the RH between 95 to 99% the value of α started decreasing, which implies that these are the delinquent points of the mixtures and that particles at the delinquent points appear to be large particles. This is because of swelling of water vapor and aging processes, exhibiting thus similar characteristics to the particles produced in arid areas [39, 40] though it can be observed that α_2 is negative and continued to increase. This shows that at delinquent points increase in the curvature of α_2 does not reflect increase in fine mode particles.

The observed variations in Ångström coefficients can be explained by changes in the effective radii of the mixtures resulting from changes in RH in the range 0% to 90%: the larger the number of small aerosol particles, the smaller the effective radius and the larger the Ångström coefficient The Ångström exponent increases with the increase in water vapor, means that the effective radius of the aerosol particles become smaller when the water vapor increases. But as from 95% to 99% RH there is an increase in fine mode particle radius which results from particle growth due to coagulation and hygroscopic growth. Coagulation rates increase as particle concentration increases (Reid et al., 1999); therefore this particle growth mechanism will be greatest at the highest optical depth (τ(λ)). Hygroscopic at high RH will also tend to increase optical depth as accumulation mode particles increase in size [41] and it reflect the occurrence of large size accumulation mode particles that may result from fine particle coagulation at high concentration from hygroscopic growth. There is also an observational evidence that Ångström exponents decrease in value as particles grow hygroscopically [42].

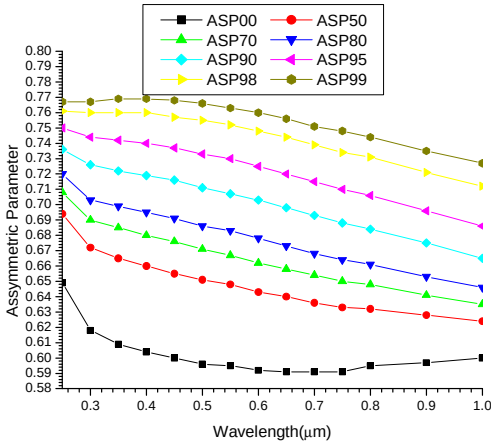

Figure 1c. A graph of asymmetric parameter against wavelength for model1 at RHs 0, 50, 70, 80, 90, 95, 98 and 99%.

The behavior of asymmetric parameter with wavelength is like power law but as it can be seen from the graph, the coefficient decreases with the increase in RH (0–90%) but becomes linear and increase with RH as from 95– 99%. The increase of asymmetric parameter with RH shows that hygroscopic growth by particles as a result of the increase in RH enhances scattering more in the forward direction of which that is why we have increase in RF(cooling) with RH.

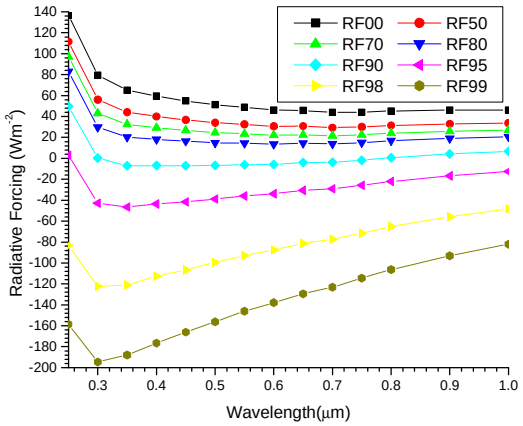

Figure 2a. A graph of radiative forcing against wavelength for model2 at RHs 0, 50, 70, 80, 90, 95, 98 and 99%.

Figure 2a is similar to figure 1a with respect to wavelengths, but the main difference is that RF(cooling) has increased with respect to RHs.

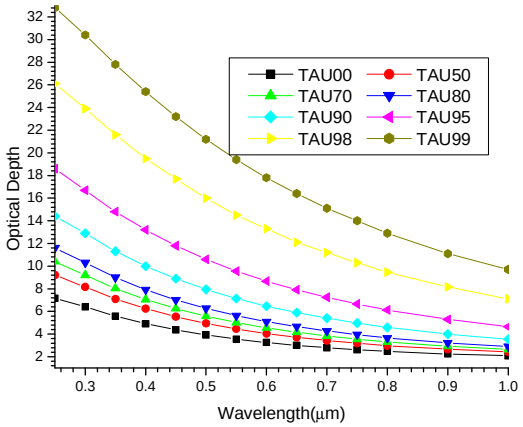

Figure 2b. A graph of optical depth against wavelength for model2 at RHs 0, 50, 70, 80, 90, 95, 98 and 99%.

Figure 2b is similar to figure 1b with respect to wavelength, but there is an increase of optical depths with the increase in RHs.

Table 3 The results of the Angstrom coefficients for Model2 using equations (4) and (5) at the respective relative humidities using regression analysis with SPSS16.0.

Linear				Quadratic			
RH(%)	R^2	α	β	R^2	α_1	α_2	β
0	0.99752	0.93799	2.03695	0.99760	-0.96661	-0.02099	2.02427
50	0.99728	1.00504	2.42128	0.99845	-1.12277	-0.08636	2.35989
70	0.99653	1.02583	2.67734	0.99875	-1.19143	-0.12148	2.58234
80	0.99555	1.03839	2.96303	0.99901	-1.24735	-0.15328	2.83099
90	0.99276	1.04410	3.70803	0.99939	-1.33552	-0.21378	3.47963
95	0.98849	1.02339	4.97507	0.99968	-1.39544	-0.27293	4.58721
98	0.98106	0.95680	7.79292	0.99989	-1.40974	-0.33226	7.05971
99	0.97493	0.89298	10.7556	0.99995	-1.38174	-0.35855	9.66779

Comparing Tables 2 and 3 shows that there is an increase in both α andα_2 , except that α_2 at 0% RH has changed sign from positive in table 2 to negative in this table.

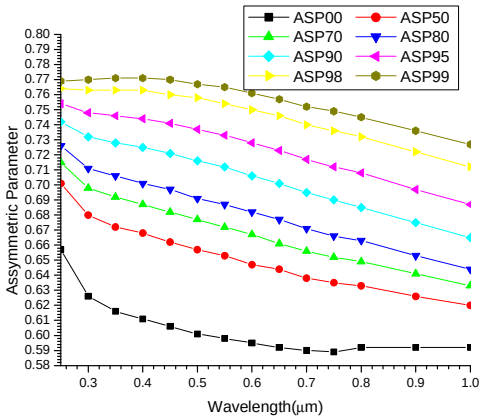

Figure 2c. A graph of asymmetric parameter against wavelength for model2 at RHs 0, 50, 70, 80, 90, 95, 98 and 99%.

Figure 2c's relation with wavelength it is similar to that of Figure 1c. but in relation to RH it shows a slight increase.

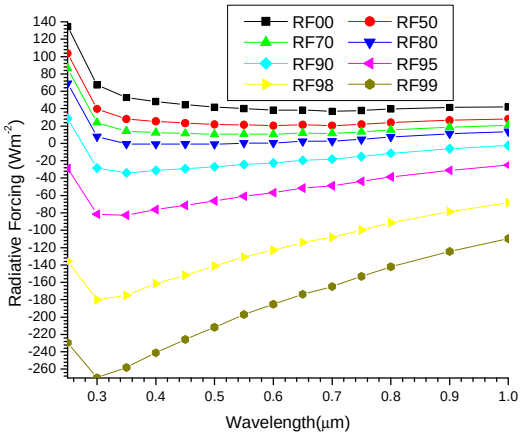

Figure 3a. A graph of radiative forcing against wavelength for model3 at RHs 0, 50, 70, 80, 90, 95, 98 and 99%.

Figure 3a is similar to Figures 1a and 2a with respect to wavelength, but the RF(cooling) is higher than both with respect to RHs.

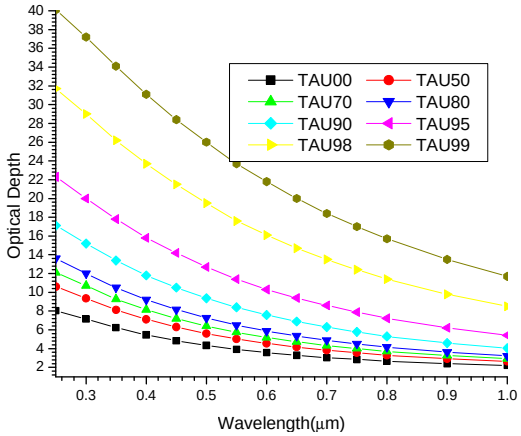

Figure 3b. A graph of optical depth against wavelength for model3 at RHs 0, 50, 70, 80, 90, 95, 98 and 99%.

Figure 3b is similar to Figures 1b and 2b with respect to wavelength, but there is an increase of optical depth with respect to RHs.

Table 4 The results of the Angstrom coefficients for Model3 using equations (4) and (5) at the respective relative humidities using regression analysis with SPSS16.0.

Linear				Quadratic			
RH(%)	R^2	α	β	R^2	α_1	α_2	β
0	0.99752	0.97817	2.17621	0.99792	-1.04481	-0.04888	2.14480
50	0.99670	1.04467	2.65697	0.99873	-1.20585	-0.11824	2.56516
70	0.99566	1.06295	2.97715	0.99900	-1.27306	-0.15413	2.84376
80	0.99445	1.07225	3.33467	0.99923	-1.32618	-0.18628	3.15496
90	0.99143	1.07173	4.26453	0.99954	-1.40306	-0.24305	3.96716
95	0.98697	1.04311	5.84636	0.99978	-1.44912	-0.29784	5.35079
98	0.97953	0.96733	9.36627	0.99993	-1.44427	-0.34987	8.44072
99	0.97340	0.89938	13.06814	0.999974	-1.40703	-0.37240	11.69813

Comparing with table3, it can be observed that both α and α_2 have increased.

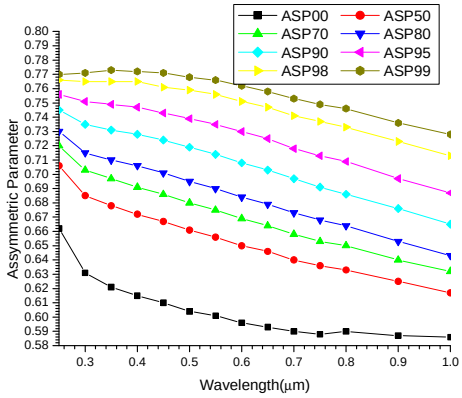

Figure 3c. A graph of asymmetric parameter against wavelength for model3 at RHs 0, 50, 70, 80, 90, 95, 98 and 99%.

In relation to wavelength Figure 3c is similar to those of Figures 1c and 2c, but its relation with RH shows a slight increase.

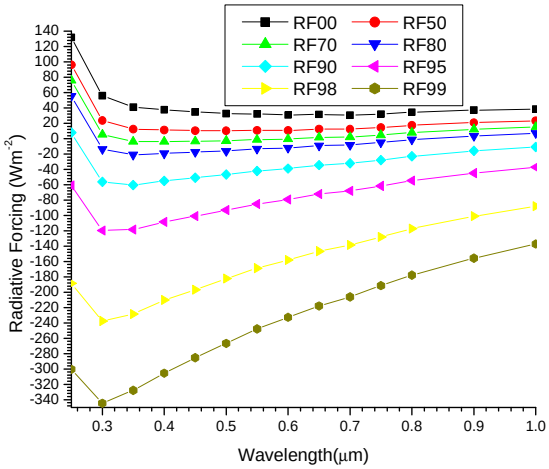

Figure 4a. A graph of radiative forcing against wavelength for model4at RHs 0, 50, 70, 80, 90, 95, 98 and 99%.

Figure 4a is similar to figure 1a, 2a and 3a with respect to wavelength, but there is an increase in RF(cooling) with the increase in RHs.

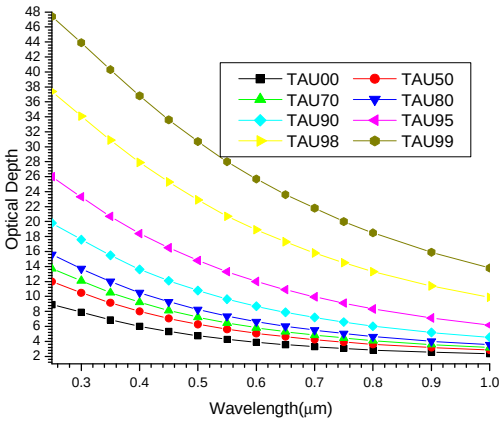

Figure 4b. A graph of optical depth against wavelength for model4at RHs 0, 50, 70, 80, 90, 95, 98 and 99%.

Figure 4b is similar to figures 1b, 2b, and 3b with respect to wavelength, but there is an increase of optical depth with the increase in RHs.

Table 5 The results of the Angstrom coefficients for Model4 using equations (4) and (5) at the respective relative humidities using regression analysis with SPSS16.0.

Linear				Quadratic			
RH(%)	R^2	α	β	R^2	α_1	α_2	β
0	0.99731	1.01207	2.31576	0.99815	-1.11236	-0.07357	2.26564
50	0.99602	1.07624	2.89341	0.99892	-1.27466	-0.14555	2.77083
70	0.99481	1.09212	3.27738	0.99917	-1.33907	-0.18115	3.10549
80	0.99350	1.09898	3.70573	0.99938	-1.38776	-0.21184	3.47947
90	0.99028	1.09243	4.82090	0.99964	-1.45523	-0.26614	4.45405
95	0.98582	1.05746	6.71730	0.99983	-1.48818	-0.31596	6.11485
98	0.97842	0.97475	10.94137	0.99995	-1.46880	-0.36242	9.82342
99	0.97236	0.90374	15.38190	0.99998	-1.42410	-0.38172	13.73121

Comparing Table 5 with Table 4, it can be observed that there is an increase in both α and α_2.

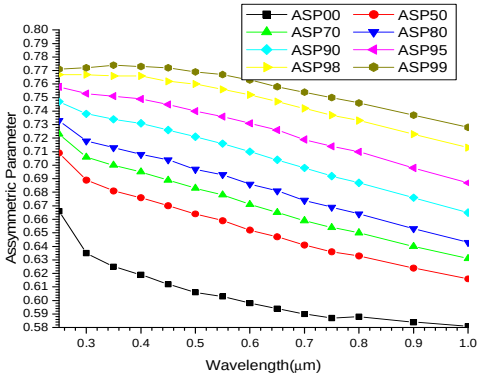

Figure 4c. A graph of asymmetric parameter against wavelength for model4

From figure 4c, the relation with wavelength is similar to that of figure 1c, 2c and 3c. but with RH it shows a slight increase.

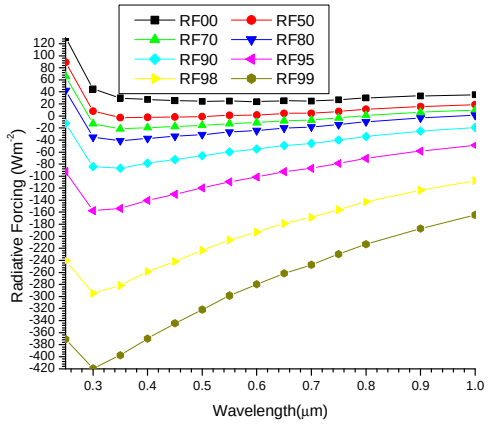

Figure 5a. A graph of radiative forcing against wavelength for model5at RHs 0, 50, 70, 80, 90, 95, 98 and 99%.

Figure 5a is similar to figures 1a 2a, 3a, and 4a with respect to wavelength, but there is an increase in RF(cooling) with the increase in RHs.

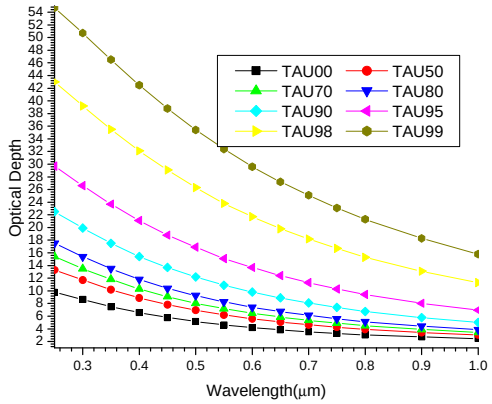

Figure 5b. A graph of optical depth against wavelength for model5at RHs 0, 50, 70, 80, 90, 95, 98 and 99%.

Figure 5b is similar to figures 1b, 2b, 3b, and 4b with respect to wavelength, but there is an increase of optical depth with the increase in RHs.

Table 6 The results of the Angstrom coefficients for Model5 using equations (4) and (5) at the respective relative humidities using regression analysis with SPSS16.0.

Linear				Quadratic			
RH(%)	R^2	α	β	R^2	α_1	α_2	β
0	0.99701	1.04109	2.45555	0.99836	-1.17169	-0.09581	2.38657
50	0.99539	1.10236	3.12990	0.99909	-1.33172	-0.16825	2.97715
70	0.99406	1.11582	3.57768	0.99930	-1.39259	-0.20303	3.36805
80	0.99264	1.12000	4.07737	0.99948	-1.43774	-0.23309	3.80431
90	0.98936	1.10842	5.37756	0.99972	-1.4958	-0.28417	4.94177
95	0.98488	1.06832	7.58854	0.99987	-1.51863	-0.33034	6.87850
98	0.97763	0.98029	12.51567	0.99997	-1.48651	-0.37135	11.20707
99	0.97161	0.90694	17.69601	0.99999	-1.43642	-0.38841	15.765599

Comparing with table 5, it can be observed that there is an increase in both α and α_2.

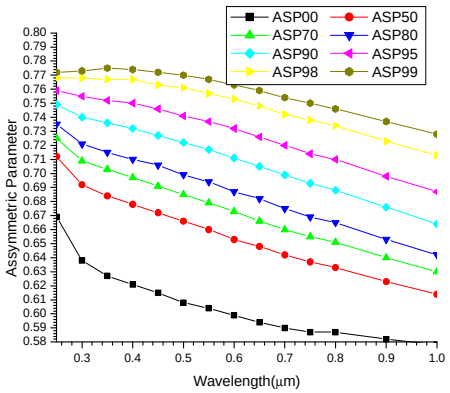

Figure 5c. A graph of asymmetric parameter against wavelength for model 5 at RHs 0, 50, 70, 80, 90, 95, 98 and 99%.

Figure 5c's relation with wavelength is similar to that of figures 1c, 2c, 3c and 4c but there is a slight increase in relation to RH.

Conclusions

From our results, we observed a slight decrease in RF(warming), with the increase in water soluble at 0% RH. But as can also be observed, the difference in the increase is becoming more noticeable as the RH increases most especially as from 50% RH. This is attributed to the increase in scattering because of the high hygroscopicity of the WS. This shows that RH has a great influence on RF in urban areas where they have diesel-fueled mobile sources, the numerous coal-fired industries and power generation stations are expected to be cooling with the increase in these activities.

Additionally, the increase in α together with the decrease in the curvature from α_2 at 0% from tables 2 and 3 together with the subsequent increase in magnitude of α_2 for the remaining tables reflect the increase in fine particles which implies that water soluble are fine particles. Also according to [36], the absolute value of the coefficient α_1 decreases with increasing particle size for fine monomodal aerosols, but in our case it is observed that α_1 increases with the increase in RHs, so we assume that the particles have bimodal type of particle size distributions with the dominance of fine particles.

Also since forward scattering strength is correlated with particles size, the value of g can also be used as a general indicator for particle size.

Additionally it can be observed that the increase in WS has lowered the deliquescent points, because at models 1 and 2, it started from 95, while models 3, 4 & 5 at 90.

Finally it can be observed that the change in Ångström coefficient due to variation in RH is comparable to that caused by change in the aerosol mixture compositions.

References

[1] Verma, S., Boucher, O., Reddy, M. S., Upadhyaya, H. C., Van, P. L., Binkowski, F. S and Sharma, O. P (2012): Tropospheric distribution of Sulphate aerosols mass and number concentration during INDOEX-IFP and its transport over the India Ocean: a GCM study.

[2] Charlson, R.J., Schwartz, S.E., Hales, J. M., Cess, R. D., Coakley, J. A., Hansen, J. E and Hotmann, D. J (1992) Climate forcing by anthropogenic aerosols, Science 255, 423-430

[3] Kiehl, J. T and Briegleb, B. P (1993) The relative role of sulphate aerosols and greenhouse gases in climate forcing. Science, 260, 311-314.

[4] Barth, M. C and Church, A. T (1999) Regional and Global distributions and lifetimes of sulphate aerosols from Mexico city and Southeast China. Journal of Geophysical Research ., 104, 30231-30239

[5] Ramanathan, V., Crutzen, P. J., Lelieveld, J., Althausen, D., Anderson, J., Andreae, M. O., Cantrell, W., Cass, G., Chung, C. E., Clarke, A. D., Collins, W.D., Coakley, J. A., Dulac, E., Heintzenberg, J., Heymsfield, A. J., Holben, B., Hudson, J., Jayaraman, A.,Kiehl, J. T ., Krishnamurti, T.N., Lubin, D., Mitra, A. P., Mac Farquhar, G., Novakov, T., Ogren, J. A., Podgorny, I. A., Prather, K., Prospero, J. M., Priestley, K., Quinn, P. K., Rajeev, K., Rasch, P., Rupert, S., Sadourny, R., Satheesh, S. K., Sherdan, P., Shaw, G. E., and Valero, F.P.J (2001) The India ocean experiment: An integrated analysis of the climate forcing and effects of the great Indo-Asia haze, Journal of Geophysical Research 106, 28371-28398.

[6] Mallet, M., Roger, J. C., Depiau, S., Putaud, J. P and Dubovik, O (2004) A study of the mixing state of black carbon in urban zone. Journal of Geophysical Research109,D0402.

[7] Brock, C. A., et al. (2003), Particle growth in urban and industrial plumes in Texas, J. Geophys. Res. , 108(D3), 4111, doi:10.1029/2002JD002746.

[8] Bates, T. S., et al. (2008), Layer aerosol chemistry during TexAQS/GoMACCS 2006: Insights into aerosol sources and transformation pro-cesses, J. Geophys. Res. , 11 3, D00F01, doi:10.1029/2008JD010023.

[9] Hess M., Koepke P., and Schult I (May 1998), Optical Properties of Aerosols and Clouds: The Software Package OPAC, Bulletin of the A merican Met. Soc. **79**, 5, p831-844.

[10] Waggoner, A. P., Weiss, R. E., Ahlquist, N. C., Covert, D. S., Will, S., and Charlson, R. J.: Optical characteristics of atmospheric aerosols, Atmos. Environ., 15, 1891–1909, 1981.

[11] Haywood, J. and Boucher, O.: Estimates of the direct and indi-rect radiative forcing due to tropospheric aerosols: a review, Rev. Geophys., 38, 513-543, 2000.

[12] Alados-Arboledas, L., Lyamani, H., and Olmo, F. J.: Aerosol size properties at Armilla, Granada (Spain), Q. J. Roy. Meteor. Soc., 129, 1395–1413, 2003.

[13] Alados-Arboledas, A., Alc´antara, A., Olmo, F. J., Mart´ınez-Lozano, J. A., Estell´es, V., Cachorro, V., Silva, A. M., Horvath, H., Gangl, A., D´ıaz, A., Pujadas, M., Lorente, J., Labajo, A., Sorribas, M., and Pavese, G.: Aerosol columnar properties retrieved from Cimel radiometers during VELETA 2002, Atmos. Environ., 42, 2630–2642, 2008.

[14] Ogren, J. A. and Charlson, R. J.: Implications for models and measurements of chemical inho-mogeneities among cloud droplets, Tellus, 44B, 489–504, 1992.

[15] IPCC (2007), Climate Change 2007:Th e Physical Science Basis . Contribution of Working Group I to the Fourth Assessment Report of the Intergovernmental Panel on Climate Change, edited by S. Solomon et al., Cambridge Univ. Press, Cambridge, U. K.

[16] Mikhailov, E. F., Vlasenko, S. S., Podgorny, I. A., Ramanathan, V., and Corrigan, C. E.: Optical properties of soot-water drop agglomerates: An experimental study, J. Geophys. Res.-Atmos., 111, D07209, doi:10.1029/2005Jd006389, 2006.

[17] Garland, R. M., Ravishankara, A. R., Lovejoy, E. R., Tol-bert, M. A., and Baynard, T.: Parameterization for the relative humidity dependence of light extinction: Organic-ammonium sulfate aerosol, J. Geophys. Res.-Atmos., 112, D19303, doi:10.1029/2006JD008179, 2007.

[18] Chylek, P., and J. Wong (1995), Effect of absorbing aerosols on global radiation bud get, Geophys . Res. Lett. , 22(8), 929 – 931, doi: 10.1 029/95GL00800.

[19] Penner, J. E., Dickinson, R. E. and O'Neil, C. A. (1992). Effects of aerosol from biomass burning on the global radiation budget. Science, 256, 1432-1434.

[20] Segan, C. and Pollack, J. (1967). Anisotropic nonconservative scattering and the clouds of Venus. J. Geophys. Res. 72, 469-477.

[21] Ångström, A.K. (1961). Techniques of Determining the Turbidity of the Atmosphere. Tellus XIII: 214.

[22] Liou K. N.(2002) An Introduction to Atmospheric Radiation, 2nd ed. Academic, San Diego, Calif.,.

[23] O'Neill, N. and Royer, A.(1993): Extraction of bimodal aerosol size distribution radii from spectral and angular slope Angstrom coefficients, Appl. Opt., 32, 1642–1645.

[24] Ranjan, R.R., Joshi, H.P. and Iyer, K.N. (2007). Spectral variation of total column aerosol optical depth over Rajkot: A tropical semi-arid Indian station. Aerosol Air Qual. Res. 7: 33-45.

[25] King, M. D. and Byrne, D. M.: A method for inferring total ozone content from spectral variation of total optical depth obtained with a solar radiometer, J. Atmos. Sci., 33, 2242–2251, 1976.

[26] Eck, T. F., Holben, B. N., Reid, J. S., Dubovic, O., Smirnov, A., O'Neil, N. T., Slutsker, I., and Kinne, S.: Wavelength dependence of the optical depth of biomass burning, urban, and desert dust aerosols, J. Geophys. Res., 104(D24), 31 333–31 349, 1999.

[27] Eck, T. F., Holben, B. N., Dubovic, O., Smirnov, A., Slutsker, I., Lobert, J. M., and Ramanathan, V.: Column-integrated aerosol optical properties over the Maldives during the northeast mon-soon for 1998–2000, J. Geophys. Res., 106, 28 555–28 566, 2001a.

[28] Eck, T. F., Holben, B. N., Ward, D. E., Dubovic, O., Reid, J. S., Smirnov, A., Mukelabai, M. M., Hsu, N. C., O' Neil, N. T., and Slutsker, I.: Characterization of the optical properties of biomass burning aerosols in Zambia during the 1997 ZIBBEE field campaign, J. Geophys. Res., 106(D4), 3425–3448, 2001b.

[29] Eck, T. F., Holben, B. N., Ward, D. E., et al.: Variability of biomass burning aerosol optical characteristics in southern Africa during SAFARI 2000 dry season campaign and a comparison of single scattering albedo estimates from radiometric measurements, J. Geophys. Res., 108(D13), 8477, doi:10.1029/2002JD002321, 2003

[30] Kaufman, Y. J., Aerosol optical thickness and atmospheric path radiance, J. Geophys. Res., 98, 2677-2992, 1993.

[31] O'Neill, N. T., Dubovic, O., and Eck, T. F.(2001a): Modified˚ Angstr¨ om exponent for the characterization of submicrometer aerosols, Appl. Opt., 40(15), 2368–2375.

[32] O'Neill, N. T., Eck, T. F., Smirnov, A., Holben, B. N., and Thulasiraman, S.: Spectral dis-crimination of coarse and fine mode optical depth, J. Geophys. Res., 198(D17), 4559, doi:101029/2002JD002975, 2003.

[33] Pedros, R., Martinez-Lozano, J. A., Utrillas, M. P., Gomez-Amo, J. L., and Tena, F.(2003): Column-integrated aerosol, optical properties from ground-based spectroradiometer measurements at Barrax (Spain) during the Digital Airborne Imaging Spectrometer Experiment (DAISEX) campaigns, J. Geophys. Res., 108(D18), 4571, doi:10.1029/2002JD003331,.

[34] Kaskaoutis, D. G. and Kambezidis, H. D.(2006): Investigation on the wavelength dependence of the aerosol optical depth in the Athens area, Q. J. R. Meteorol. Soc., 132, 2217–2234,.

[35] Reid, S. J., Eck T. F., Christopher S. A., Hobbs P. V. and Holben B.,(1999) Use of Angtrom exponent to estimate the variability of optical and physical properties of aging smoke particles in Brazil, J. Geophys. Res. 104(D22), 27, 473—27, 489.

[36] Schuster, G. L., Dubovik, O., and Holben, B. N.:Angstrom exponent and bimodal aerosol size distributions, J. Geophys. Res., 111, D07207, doi:101029/2005JD006328, 2006.

[37] Tang, I. N. (1996). Chemical and size effects of hygroscopic aerosols on light scattering coefficients. Journal of Geophysical Research, 101, 19245–19250.

[38] Fitzgerald, J. W. (1975) Approximation formulas for the equilibrium size of an aerosol particle as a function of its dry size and composition and ambient relative humidity. J. Appl. Meteorol., 14, 1044 –1049

[39] Kaskaoutis D. G., Kambezidis H. D., Hatzianastassiou N., Kosmopoulos P. G., and Badarinath K. V. S. (2007a) Aerosol climatology: dependence of the Angstrom exponent on wavelength over four AERONET sites, Atmos. Chem. Phys. Discuss., 7, 7347–7397.

[40] Kaskaoutis, D. G., Kambezidis, H. D., Hatzianastassiou, N., Kosmopoulos, P. G., & Badarinath, K. V. S. (2007b). Aerosol climatology: On the discrimination of aerosol types over four AERONET sites. Atmospheric Chemistry and Physical Discussion, 7,6357−6411.

[41] Eck, T. F., Holben, B. N., Dubovic, O., Smirnov, A., Goloub, P., Chen, H. B., Chatenet, B., Gomes, L., Zhang, X. Y., Tsay, S. C., Ji, Q., Giles, D., and Slutsker, I.: Columnar aerosol optical properties at AERONET sites in central eastern Asia and aerosol transport to the tropical mid-Pacific, J. Geophys. Res., 110, D06202, doi:10.1029/2004JD005274, 2005.

[42] Carrico, C.M., Rood, M.J., Ogren, J.A., (1998): Aerosol light scattering properties at Cape Grim, Tasmania, during the First Aerosol Characterization Experiment (ACE 1), J. Geophys. Res., 103, 16565-16574.